Reaction Chemistry & Engineering

ROYAL SOCIETY OF CHEMISTRY

PAPER

View Article Online
View Journal | View Issue



Cite this: *React. Chem. Eng.*, 2021, **6**, 1974

# Dynamics of phase transitions in $Na_2TiO_3$ and its possible utilization as a $CO_2$ sorbent: a critical analysis

Maria Valeria Blanco, *[a] Paula Macarena Abdala, [b] Fabiana Gennari [cde] and Federico Cova *[a]

Na-Based materials are emerging as promising high-temperature $CO_2$ sorbents. In this work, we provide a detailed study on the synthesis of $Na_2TiO_3$ *via* a solid-state route using NaOH and $TiO_2$ as starting reactants. The $CO_2$ sorption properties of the synthesized $Na_2TiO_3$ were evaluated by thermogravimetric analysis. A subsequent comprehensive study on the complex reaction mechanism of $Na_2TiO_3$ at high temperatures under carbonation conditions was performed *via* real time *in situ* synchrotron X-ray diffraction analysis. *In situ* experiments performed under different conditions revealed the occurrence of thermally-driven phase transitions derived from the structural instability of the material at high temperatures. These reactions could be differentiated from carbonation processes, allowing the proposal of a reaction mechanism of the material as a $CO_2$ sorbent. The obtained results can explain the abnormal dynamic thermogram displayed by $Na_2TiO_3$ in the presence of $CO_2$ within a temperature range that is of interest for practical applications and serve as a basis for evaluating the feasibility of using this material in $CO_2$ capture schemes.

Received 31st March 2021,
Accepted 13th July 2021

DOI: 10.1039/d1re00125f

rsc.li/reaction-engineering



## 1 Introduction

Global $CO_2$ emissions have increased by about 90% in the last 50 years, with industrial processes and fossil fuel combustion being the two major contributors, and about 78% of the total increment having occurred in the period from 1970 to 2011.[1] Since $CO_2$ has been pointed out as mainly responsible for the greenhouse effect that drives global climate change, the development of strategies for mitigating its release to the atmosphere constitutes an essential prerequisite to prevent further global warming. A closer look into anthropogenic $CO_2$ emissions shows that approximately 40% of them are generated by power plants.[2] Hence, the design and engineering of materials and processes to capture and retain the $CO_2$ before its release to the atmosphere appear as a viable alternative to tackle climate change, while transitioning to more sustainable and renewable power schemes.

Solid sorbents have been proven to efficiently remove $CO_2$ from high-temperature industrial gas streams,[3–5] with promising results when implemented at a pilot scale in different coal-fired and cement plants.[6,7] Indeed, these materials with the ability to react with $CO_2$ at high temperatures have shown great potential for the separation of $CO_2$ in sorption enhanced reaction processes (SERPs) for hydrogen production, $CH_4 + 2H_2O \rightarrow CO_2 + 4H_2$,[8,9] where the *in situ* $CO_2$ removal shifts the equilibrium towards high-purity hydrogen production and increased hydrocarbon conversion. In the case of steam reforming processes (SESRs), continuous capture of $CO_2$ can dramatically enhance $H_2$ selectivity and avoid cooling processes.[10,11] Therefore, solid sorbents can be applied in either pre-combustion or post-combustion $CO_2$ capture schemes. Ideally, these materials should exhibit high sorption capacities, good regeneration capabilities and long-term stability, together with a low price.

Among proposed high-temperature solid $CO_2$ sorbents,[12] alkali and alkaline-earth oxides containing lithium, sodium, potassium, calcium and/or magnesium have shown promising properties towards $CO_2$ capture. When reacting with $CO_2$, these sorbents usually exhibit a temperature-dependent behaviour in which $CO_2$ is first chemisorbed,

[a] *European Synchrotron Radiation Facility, 71 Avenue des Martyrs, Grenoble, France. E-mail: federico.cova@csic.es*
[b] *Department of Mechanical and Process Engineering, ETH Zürich, Leonhardstrasse 21, CH-8092 Zurich, Switzerland*
[c] *Consejo Nacional de Investigaciones Científicas y Técnicas (CONICET), R8402AGP, S. C. de Bariloche, Río Negro, Argentina*
[d] *Centro Atómico Bariloche (CAB-CNEA), R8402AGP, S.C. de Bariloche, Río Negro, Argentina*
[e] *Universidad Nacional de Cuyo (UNCuyo), Instituto Balseiro, Av. Bustillo 9500, R8402AGP Bariloche, Río Negro, Argentina*

producing an external shell composed of either $Li_2CO_3$, $Na_2CO_3$, $K_2CO_3$, $CaCO_3$ or $MgCO_3$. Once the temperature is high enough to activate diffusion processes, the reaction proceeds through the bulk of the particles.

Li-Based materials, such as $Li_4SiO_4$, $Li_2ZrO_3$, $Li_5AlO_4$ and $Li_2CuO_2$, have been widely studied as $CO_2$ sorbents,[13] displaying high sorption capacities within the temperature range of 400–700 °C.[14–17] However, from a large-scale application perspective, low cost Na-based captors, such as $Na_2TiO_3$, $Na_2ZrO_3$, $Na_2SiO_3$ and $Na_4SiO_4$, are more attractive.[18–21] The lower cost is usually associated with the manufacture process since, as a general rule, lithium oxides are more expensive than their sodium counterparts. Given that Na-based sorbents, such as $Na_2ZrO_3$, can reach $CO_2$ sorption capacities very close to those of Li-based systems,[22,23] it is important to further explore their properties and capabilities towards $CO_2$ capture.

$Na_2TiO_3$ is a promising material for positive electrodes in Na-ion batteries[24–26] and has also been proposed as a possible $CO_2$ sorbent.[22,27] Interestingly, the thermogram displayed by $Na_2TiO_3$ when subjected to a $CO_2$ flow differs from those exhibited by other $CO_2$ sorbents. The $Na_2TiO_3$ thermogram shows two weight increments, which are then followed by sequential weight decrements. This experimental evidence questions the stability $Na_2TiO_3$ at high temperatures and its ability to trap $CO_2$. In addition to this, *ex situ* XRD characterization of $Na_2TiO_3$–$CO_2$ reaction products showed the formation of $Na_2CO_3$, $Na_2O$, m-$Na_4Ti_5O_{12}$, h-$Na_4Ti_5O_{12}$ and $Na_{16}Ti_{10}O_{28}$ phases.[27] The observation of these chemical species, together with the absence of $TiO_2$, is indicative of the partial reaction of $Na_2TiO_3$ with $CO_2$, and also suggests a complex temperature-dependent reaction mechanism. Despite the great effort to understand the reaction pathway of $Na_2TiO_3$–$CO_2$ at high temperatures,[27] the great likelihood of disproportionation of this material and its thermal instability makes standard characterization methods inaccurate. Instead, more sophisticated analysis tools that allow tracking in real time the structural changes occurring at high temperatures in the presence of $CO_2$ need to be employed in order to describe the reaction path and better understand the behavior of the system under operative conditions.

In this work, we present thermodynamic calculations and experimental data on the synthesis of $Na_2TiO_3$ *via* a solid-state route. Then, we show the benefits of using high temperature *in situ* synchrotron X-ray diffraction analysis to gain valuable insights on phase transformations that are difficult to detect by standard *ex situ* characterization techniques. *In situ* X-ray diffraction experiments revealed the occurrence of thermally driven structural changes of the material. These phase transformations could be differentiated from carbonation processes, allowing the proposal of a reaction mechanism of $Na_2TiO_3$ as a $CO_2$ sorbent. The influence of the surrounding atmosphere on the carbonation kinetics and reaction path of $Na_2TiO_3$ at high temperatures is discussed.

# 2 Experimental

## 2.1 Material synthesis

Sodium hydroxide (millimeter spheres of NaOH, Biopack, purity 98%) and titanium dioxide (nanopowder of $TiO_2$, Sigma, purity 99%, anatase ≈75 wt% and rutile ≈25 wt%) were used as starting materials. The synthesis of β-$Na_2TiO_3$ was performed as follows. A mixture of NaOH–$TiO_2$ with a 2.1 : 1 molar ratio was handled in an Ar-filled glove box and introduced into a milling chamber. The powder mixture was then milled in a planetary ball mill (Fritsch Pulverisette P6) for 15 min in an Ar atmosphere. The selected milling conditions included a ball to powder ratio of 40 : 1 and 400 rpm. After milling, the powders were pressed and heated in air at 800 °C for 5 h.

## 2.2 Thermodynamic calculations

The equilibrium composition of the 2NaOH–$TiO_2$ mixture as a function of temperature was calculated by a Gibbs free energy minimization method using HSC software (6.1 version).[28] This method determines the equilibrium products at different temperatures and pressures for a heterogeneous system based on an extensive thermochemical database which contains enthalpy, entropy and heat capacity data of chemical compounds. The reaction system was specified in terms of the number of phases, species and the initial amount of reactants. The starting reaction system was composed of 2 kmol NaOH and 1 kmol $TiO_2$ (75% anatase and 25% rutile) in the solid phase, and air ($N_2$ = 78 kmol and $O_2$ = 21 kmol $O_2$) in the gas phase. The presence of $H_2O$(l,g) was also contemplated. Several species were considered as possible in the solid phase: NaOH·$H_2O$; $Na_2O$; Na; NaH; $Ti_3O_2$; $Ti_2O_3$; $Na_2O_2$; $Na_2TiO_3$ (beta phase); $Na_2Ti_2O_5$; $Na_2Ti_3O_7$; $Na_2Ti_6O_{13}$. Some sodium titanates ($Na_4Ti_5O_{12}$, $Na_{16}Ti_{10}O_{28}$) previously reported were not included in the equilibrium composition calculations because of the lack of thermodynamic properties reported in the literature. Calculations were carried out in the temperature range of 0–800 °C and at 1 atm.

## 2.3 Characterization techniques

The structural and thermal properties of the samples were studied using X-ray powder diffraction (XRPD, Bruker D8 Advance) and simultaneous thermogravimetry and differential scanning calorimetry (TG-DSC, Linseis STA PT1600) coupled with mass spectroscopy (MS, ThermoStar Pfeiffer). *Ex situ* XRPD patterns were collected in the 2$\theta$ range of 10–80° with CuKα radiation, a voltage of 40 kV and an electric current of 40 mA. The thermal behaviour of the as-milled 2NaOH–$TiO_2$ mixture was measured with a heating rate of 5 °C $min^{-1}$ from room temperature to 800 °C under a synthetic air flow (50 $cm^3$ $min^{-1}$ STP). Dynamic $CO_2$ capture measurements were carried out with a thermogravimetric instrument (TG-HP50, TA Instruments). The as-synthesized β-$Na_2TiO_3$ was heated from room temperature to 800 °C at a

heating rate of 5 °C $min^{-1}$ using a $CO_2$ flow rate of 50 $cm^3$ $min^{-1}$ (STP).

*In situ* synchrotron X-ray diffraction (XRD) measurements were performed at the beamline ID31 of the European Synchrotron Radiation Facility (ESRF). For this, β-$Na_2TiO_3$ samples were loaded into 1 mm outer diameter quartz capillaries and then subjected to different treatments: 1) dynamic heating under a $N_2$ gas flow up to a final temperature of 615 °C, and then switching the gas to $CO_2$ and maintaining isothermal conditions for 1 h; 2) heating under a $N_2$ gas flow up to 770 °C and then switching the gas to $CO_2$ and maintaining isothermal conditions for 1 h; 3) heating under a $CO_2$ gas flow up to 770 °C and maintaining isothermal conditions. In all cases, the heating ramp was 5 °C $min^{-1}$. A sketch of the experimental setup can be found elsewhere.[29] *In situ* synchrotron X-ray diffraction data were collected using a PerkinElmer detector, at a wavelength of 0.1771 Å and with a beamsize of 0.6 mm × 0.6 mm ($V \times H$). Each frame was collected with an exposure time of 1 s. Data were processed using the pyFAI package.[30] The analysis of selected diffraction peaks representative of different crystallographic phases was performed by curve fitting with the Gaussian function, using Fityk software.[31] Rietveld refinements were performed using GSAS II software.[32]

# 3 Results and discussion

## 3.1 Synthesis and $CO_2$ properties of the β-$Na_2TiO_3$ system

**3.1.1 Study of the thermal behaviour of 2NaOH–$TiO_2$ mixtures.** The equilibrium composition of the 2NaOH–$TiO_2$ system was estimated based on the Gibbs energy minimization method.[28] The thermodynamic calculations displayed in Fig. 1 predict the complete consumption of $TiO_2$ at 0 °C, simultaneous with the formation of β-$Na_2TiO_3$ and $H_2O$(l,g) as the main reaction products.

The hydration of NaOH to NaOH·$H_2O$ at temperatures lower than 100 °C is promoted by the $H_2O$ formation. A progressive temperature rise to 300 °C increases the amounts of both β-$Na_2TiO_3$ and $H_2O$(g), reaching for each phase a maximum amount that remains constant for higher temperatures. From the previous interpretations, it is possible to infer that the formation of β-$Na_2TiO_3$ is favored thermodynamically by heating of the starting mixture in air. The expected reaction at room temperature can be expressed as:

$$2NaOH(s) + TiO_2(s) \rightarrow Na_2TiO_3(s) + H_2O(g) \quad (1)$$

where $\Delta G°$ (293 K) = −44.75 kJ $mol^{-1}$ which is thermodynamically favorable.

From the thermodynamic calculations, it is expected that the both formation of $Na_2Ti_2O_5$ and β-$Na_2TiO_3$ will occur simultaneously from 0 °C; however, the $Na_2Ti_2O_5$ amount decreases to a minimum value with the temperature rising to 200 °C. A possible formation reaction is:

$$2NaOH(s) + 2TiO_2(s) \rightarrow Na_2Ti_2O_5(s) + H_2O(l,g) \quad (2)$$

As the temperature increases from 0 °C, $Na_2Ti_2O_5$ is the only titanium source to induce the production of an extra amount of β-$Na_2TiO_3$, consuming NaOH:

$$2NaOH(s) + Na_2Ti_2O_5(s) \rightarrow 2Na_2TiO_3(s) + H_2O(g) \quad (3)$$

Reactions (2) and (3) are also thermodynamically favorable above 0 °C and 100 °C, respectively.

Previous thermodynamic analysis determined the on-going reactions in the absence of any restrictions caused by kinetics and/or transport phenomena and can serve as a benchmark to compare with the experimental results. In order to evaluate the reactivity of the 2NaOH–$TiO_2$ mixture for the synthesis of β-$Na_2TiO_3$, TG-DSC measurements were combined with MS analysis (Fig. 2). The TG curve of the as-milled 2NaOH–$TiO_2$ powder shows a sharp weight loss of 13% between 50 and 200 °C, which correlates with an endothermic peak in the DSC curve. According to MS analysis, this sharp weight loss can be

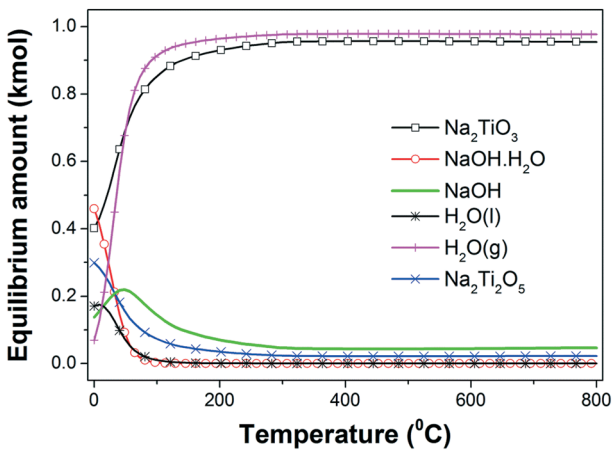


Fig. 1 Equilibrium amount (kmol) of different species in the 2NaOH–$TiO_2$ system as a function of temperature at 1 atm.

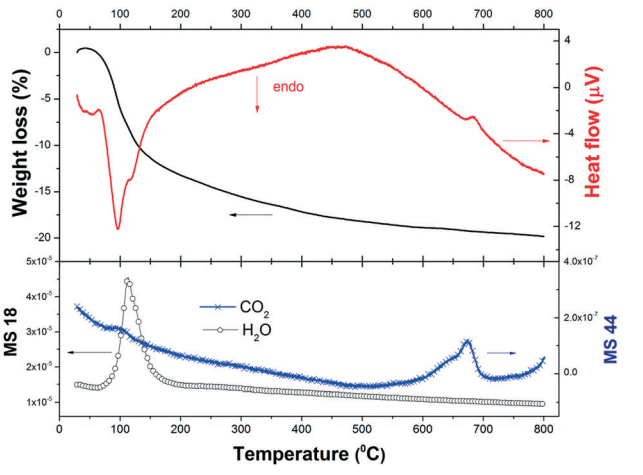


Fig. 2 Weight loss (in%), heat flow (μ V) and gas evolved ($H_2O$ and $CO_2$) during heating of as-milled 2NaOH–$TiO_2$ in synthetic air.

ascribed mainly to water evolution due to the formation of $Na_2TiO_3$ (reaction (1), theoretical value of 11.3%) and also attributable to dehydration from pre-adsorbed water on NaOH. As the temperature increases up to 800 °C, the weight loss progresses to 20% and MS analysis evidences gradual water and $CO_2$ evolution. In the DSC curve, no melting of pure NaOH or melting of the NaOH–$Na_2CO_3$ eutectic mixture[33] was observed. These events are expected at about 320 °C and 282 °C, respectively. Their absence indicates that NaOH was completely consumed at temperatures lower than 282 °C and/or NaOH partially reacted with $CO_2$ present in the air during handling, forming $Na_2CO_3$.[34] $CO_2$ detection by MS reveals $CO_2$ release, evidenced by the occurrence of: a small bump at 100 °C, a gradual decline observed in the curve starting from low temperatures, and a peak between 600 and 700 °C. These events indicate that slight $CO_2$ adsorption occurred prior to the thermal analysis run. Additionally, an exothermic peak at 685 °C was identified and is analyzed in the following paragraph.

The *ex situ* XRPD patterns of the products obtained at different reaction temperatures are displayed in Fig. 3. As reference, the XRPD patterns of nano-$TiO_2$ and as-milled 2NaOH–$TiO_2$ powders are also included (Fig. 3a and b). After milling, the anatase and rutile phases of $TiO_2$ remain, while $Na_2CO_3$ is formed due to carbonation of NaOH during the XRD measurement in air (Fig. 3b). Thus, milling processes promote a high degree of mixing of the starting reactants, independent of the starting size of the powders. Heating at 650 °C induces the formation of α-$Na_2TiO_3$ (Fig. 3c) simultaneous with minor $CO_2$ release, as inferred from the TG curve. The most intense diffraction peaks of $Na_2CO_3$ are still detected, with very low intensity. At 800 °C, the main phase obtained is β-$Na_2TiO_3$ with $Na_{16}Ti_{10}O_{28}$ (Fig. 3d). Prolonged heating at 800 °C favors the complete crystallization of β-$Na_2TiO_3$ (Fig. 3e). From the XRD and TG-DSC results, it can be speculated that at 685 °C, transformation between α- and β-$Na_2TiO_3$ occurred during heating, in agreement with previous studies using fine rutile-$TiO_2$.[34]

Some correlations can be made by comparison of the TG-DSC-MS results, XRPD studies and thermodynamic calculations. TG-DSC-MS measurements show the high reactivity between NaOH and $TiO_2$ at temperatures lower than 200 °C, with $H_2O$ evolution due to reaction (1) and, as a consequence, NaOH dehydration. This reaction continues as the temperature increases, showing progressive $H_2O$ release. Similar predictions were obtained from the thermodynamic calculations up to 200 °C. However, equilibrium calculations anticipate that the reaction between NaOH and $TiO_2$ is almost completed at 300 °C, with the difference from experimental results being ascribed to kinetic factors. The tests show the formation of metastable α-$Na_2TiO_3$ at 650 °C, which transforms to β-$Na_2TiO_3$ upon heating. The phase transformation towards the formation of β-$Na_2TiO_3$ progresses during the temperature ramp up to 800 °C, however upon reaching this temperature the reaction is still incomplete and requires additional time at this temperature to achieve completion. Although α-$Na_2TiO_3$ and $Na_{16}Ti_{10}O_{28}$ were identified at different temperatures, their formation could not be derived from thermodynamic calculations due to the lack of thermochemical data. Heating for 5 h produces β-$Na_2TiO_3$ as a single phase. Therefore, nano-$TiO_2$ reacts with NaOH at the beginning of heating, producing water, forming α-$Na_2TiO_3$ as an intermediate phase and finally producing β-$Na_2TiO_3$ at 800 °C after prolonged heating.

**3.1.2 Thermogravimetric characterization of the reaction of β-$Na_2TiO_3$ with $CO_2$.** To study the $CO_2$ sorption behaviour of as-synthesized β-$Na_2TiO_3$, dynamic $CO_2$ measurements were performed. The results displayed in Fig. 4 show a continuous $CO_2$ capture up to 3.5 wt% from room temperature to 400 °C, followed by a progressive weight loss of 1.5 wt% until 600 °C. After that, a sharp $CO_2$ absorption peak was registered from 620 °C to 800 °C, with 8.0 wt% $CO_2$ captured.

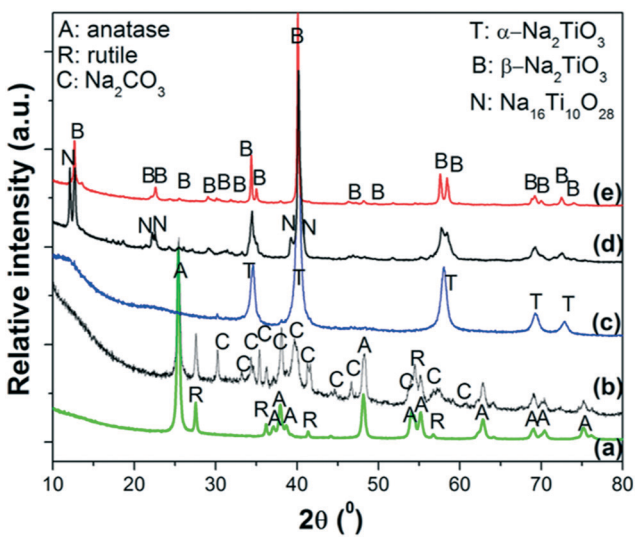


Fig. 3 XRPD patterns of: a) starting powders of nano-$TiO_2$; b) as-milled 2NaOH–$TiO_2$ mixture; heating up to c) 650 °C, d) 800 °C and e) 800 °C, 5 h. Heating ramp: 5 °C $min^{-1}$ in synthetic air.

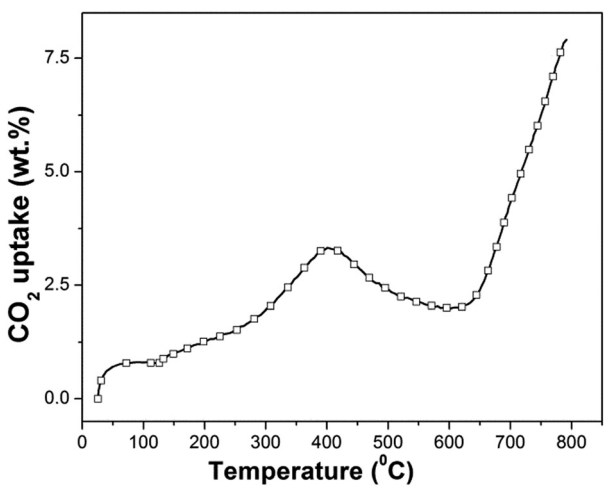


Fig. 4 Dynamic thermogravimetric analysis of synthesized β-$Na_2TiO_3$. Heating ramp: 5 °C $min^{-1}$; 50 $cm^3$ $min^{-1}$ STP of $CO_2$.

The dynamic thermogram showing a weight increment followed by a weight decrement, and a subsequent weight increment, is not in line with previous results reported for other $CO_2$ sorbents, which typically exhibit two consecutive weight increments as a function of increasing temperature (the first one is associated with $CO_2$ chemisorption and the second one is associated with $CO_2$ absorption). However, our results show similarities to the only non-isothermal previous study on $Na_2TiO_3$,[27] although there are differences in the temperature ranges where the $CO_2$ capture and weight loss were observed. In the above-mentioned report, the authors attribute the abnormal dynamic thermogram of $Na_2TiO_3$ to a different temperature-dependent $CO_2$ capture reaction mechanism, and to the poor thermal stability of the ceramic.

### 3.2 *In situ* synchrotron X-ray diffraction analysis

Three *in situ* XRD experiments were carried out with the aim of understanding: 1) the reaction mechanism of $Na_2TiO_3$ during high temperature carbonation, and 2) the effect of the initial atmosphere on the reaction path and kinetics.

The experiments involved dynamic heating under either a $N_2$ or $CO_2$ flow followed by isothermal conditions at selected temperatures under a $CO_2$ gas flow. The proposed measurements allowed distinguishing structural changes derived from the reaction of $Na_2TiO_3$ with $CO_2$ from thermally driven changes that may occur due to the instability of the material. Furthermore, the preheating of the samples under a $N_2$ flow allowed mimicking the procedure commonly used to characterize carbonation reaction products by *ex situ* methods. In this procedure, samples are first heated to a selected temperature under an inert gas atmosphere and then exposed to $CO_2$ for 1 or 2 hours. Therefore, the obtained results also will serve to visualize the limitations that these procedures might present for obtaining an accurate description of high temperature carbonation reactions. This is essential to relate chemical processes to dynamic TG $CO_2$ sorption curves.

**3.2.1 $Na_2TiO_3$ heated under $N_2$ followed by isothermal heating at 615 °C under $CO_2$.** $Na_2TiO_3$ was subjected to continuous heating at a ramp of 5 °C $min^{-1}$ under an inert gas flow up to 615 °C. Once this temperature was reached, the gas was switched to $CO_2$ and the sample was kept under isothermal conditions for 1 h. Fig. 5a displays the evolution of the X-ray diffraction patterns upon heating, and Fig. 5b shows the corresponding phase composition and temperature evolution. Interestingly, it is possible to notice that at 40 °C (initial temperature of the experiment), β-$Na_2TiO_3$ already has suffered a partial transition and the resulting material is a mixture of β-$Na_2TiO_3$, a secondary phase and a very small fraction of $Na_2CO_3$ that could be formed due to $CO_2$ chemisorption derived from air exposure. It is important to remark that the initial composition of the system is different from the one observed right after the synthesis process. The secondary phase was indexed using DICVOL06 (ref. 35) and the results showed good agreement with a monoclinic lattice having the following parameters: $a$ = 6.6651 Å, $b$ = 4.6488 Å, $c$ = 3.4209 Å and $\beta$ = 110.1°. This phase is indicated within the figures as m-$Na_2TiO_3$, and to the best of our knowledge, it has not been previously reported. The presence of the β-$Na_2TiO_3$ phase accompanying the monoclinic one hinders any attempt to determine other structural parameters of this phase, such as atomic positions. The monoclinic phase reverts to β-$Na_2TiO_3$ after reaching 300 °C, as can be seen in the patterns presented in Fig. 5a, where the characteristic reflections of the monoclinic phase, such as the peak at $2\theta$ = 5.22°, disappear. Simultaneously, the small percentage of $Na_2CO_3$ also decreases, indicating the release of $CO_2$. This is accompanied by the subtle appearance of reflections corresponding to the $Na_2O$ phase. According to

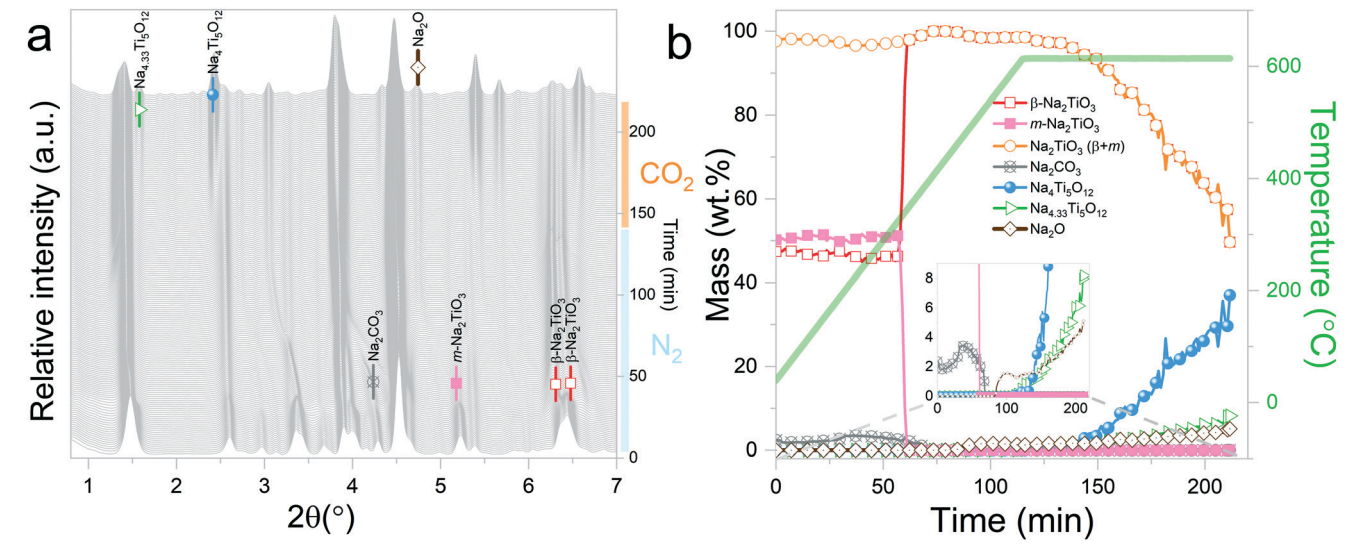


Fig. 5 $Na_2TiO_3$ heating under a $N_2$ flow until 615 °C, followed by isothermal conditions under a $CO_2$ gas flow: a) evolution of X-ray diffraction patterns upon heating; b) phase evolution (wt%) as a function of time and temperature.

Sánchez-Camacho *et al.*,[27] these results can be explained by $CO_2$ chemisorption followed by $CO_2$ release, caused by the heating, which would lead to the formation of an external shell of $Na_2O$. From the figure, it can be noticed that β-$Na_2TiO_3$ remains stable up to 600 °C under an inert atmosphere. Once the gas flow is switched to $CO_2$, β-$Na_2TiO_3$ undergoes partial decomposition into $Na_{4.33}Ti_5O_{12}$ (01-084-8819 PDF file) and $Na_4Ti_5O_{12}$ (00-052-1814 PDF file). The disproportionation follows reactions (4) and (5), respectively.

$$5Na_2TiO_3 \rightarrow Na_{4.33}Ti_5O_{12} + 2.835Na_2O + 0.0825O_2 \quad (4)$$

$$5Na_2TiO_3 \rightarrow Na_4Ti_5O_{12} + 3Na_2O \quad (5)$$

Sánchez-Camacho *et al.*[27] propose reaction (6) as an intermediary step for reaction (5), suggesting that $Na_2CO_3$ is not observed because it immediately decomposes following reaction (7).

$$5Na_2TiO_3 + 3CO_2 \rightarrow 3Na_2CO_3 + Na_4Ti_5O_{12} \quad (6)$$

$$Na_2CO_3 \rightarrow CO_2 + Na_2O_{(sub)} \quad (7)$$

**3.2.2 $Na_2TiO_3$ heated under $N_2$ followed by isothermal heating at 770 °C under $CO_2$.** $Na_2TiO_3$ was heated to 770 °C at a ramp of 5 °C $min^{-1}$ under an inert gas flow. At 770 °C, the gas was switched to $CO_2$ and the sample was kept under isothermal conditions for 1 h. The initial diffractograms for this measurement (Fig. 6a) display a similar phase mixture to the previous one (Fig. 6b) with a difference in composition of 2%, which is well within the margin of error. As expected, the sample follows the same path as the previous one until around 630 °C. At this temperature, β-$Na_2TiO_3$ decomposes showing the appearance of a new phase, which is similar to the $Na_{16}Ti_{10}O_{28}$ structure previously reported by Mayer and Perez[36] (01-076-0686 PDF file). This phase was also observed by Sánchez-Camacho *et al.*[27] However, the intensity ratios between some reflections do not match the expected values. This could be an indication of an isostructural phase with a slightly different composition. Unfortunately, the presence of secondary phases makes it difficult to determine the exact difference in the stoichiometry. A proposed reaction mechanism is presented in eqn (8).

$$10Na_2TiO_3 \rightarrow Na_{16}Ti_{10}O_{28} + 2Na_2O \quad (8)$$

Interestingly, it should be noticed that in the previously mentioned work, the proposed reaction pathway considers β-$Na_2TiO_3$ carbonation as an intermediary step for reaction (8). However, our results show that reaction (8) occurs even in the absence of $CO_2$. The results from these measurements also confirm the proposition of Sánchez-Camacho[27] regarding eqn (6) being a required intermediary step for reaction (5), since this decomposition to $Na_4Ti_5O_{12}$ is not observed under a $N_2$ flow. Peaks belonging to $Na_2O$ can also be observed up to 770 °C, the temperature at which the sample atmosphere is changed to $CO_2$. At this stage, new reflections emerge, indicating the formation of an additional phase. The new peaks were indexed to the $Na_{0.97}Ti_2O_4$ phase (04-014-7035 PDF file). Since this transition only occurs in the presence of a $CO_2$ gas flow, it is possible to assume that $Na_2CO_3$ plays a role as an intermediate product of this decomposition. A possible reaction path is presented in eqn (9).

$$2Na_{16}Ti_{10}O_{28} + 11.15CO_2 \rightarrow 10Na_{0.97}Ti_2O_4 + 11.15Na_2CO_3 + 2.425O_2 \quad (9)$$

**3.2.3 $Na_2TiO_3$ heated under $CO_2$ followed by isothermal heating at 770 °C.** β-$Na_2TiO_3$ was heated at a ramp of 5 °C $min^{-1}$ under a $CO_2$ gas flow, until reaching a temperature of 770 °C. Once this temperature was reached, the sample was

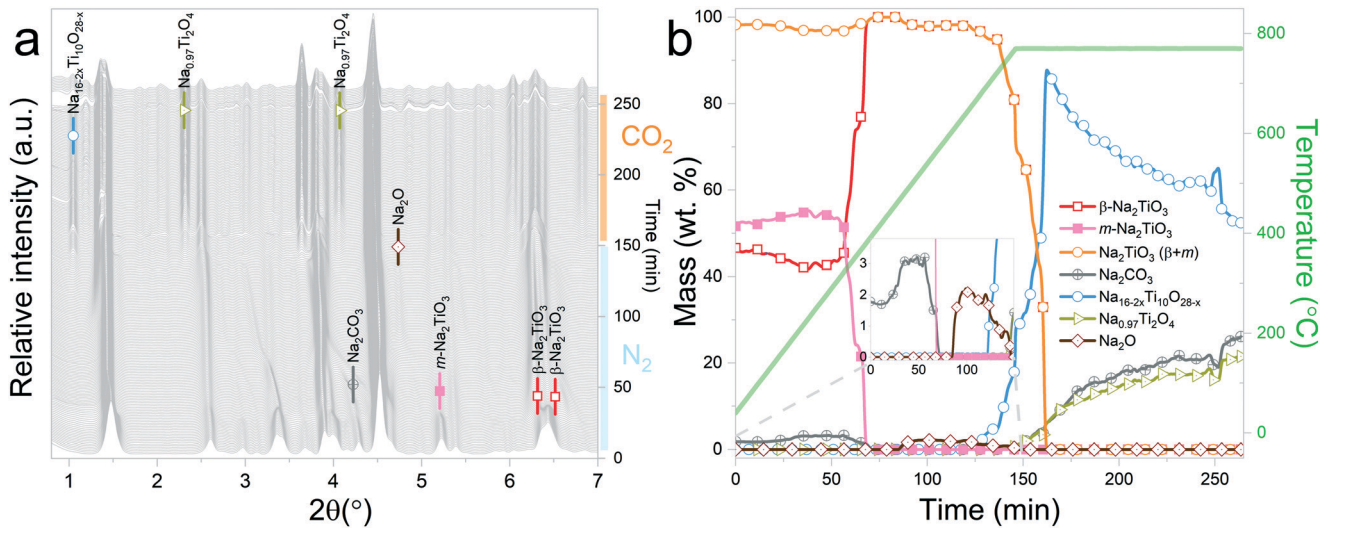


Fig. 6 $Na_2TiO_3$ heating under a $N_2$ flow until 770 °C, followed by isothermal conditions under a $CO_2$ gas flow: a) evolution of X-ray diffraction patterns upon heating; b) phase evolution (wt%) as a function of time and temperature.

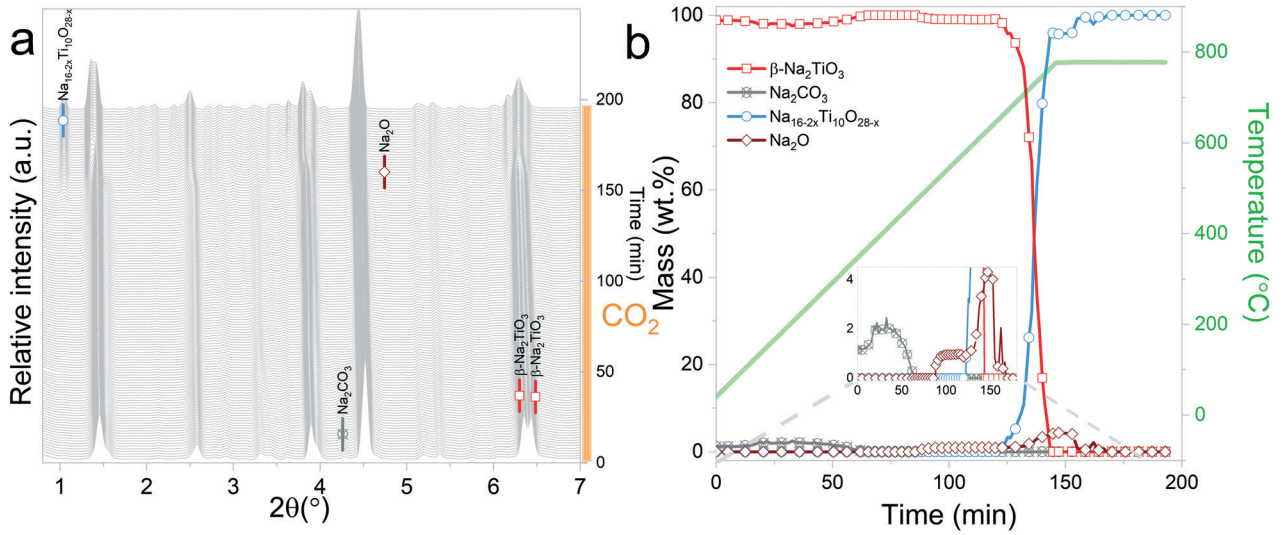


Fig. 7 $Na_2TiO_3$ heating under a $CO_2$ gas flow, followed by isothermal conditions at 770 °C: a) evolution of X-ray diffraction patterns during heating; b) phase evolution (wt%) as a function of time and temperature.

kept under isothermal conditions. As it can be observed from Fig. 7a and b, the phase composition of the starting material differs from the ones observed in the previous measurements, in which the heating process was performed under an inert gas flow. In this case, the sample exhibits almost pure β-$Na_2TiO_3$. Although the reason for this is not clear, it could be speculated that the presence of $CO_2$ inhibits the growth of the monoclinic phase.

At the initial stages of heating, the XRD patterns display an almost negligible amount of $Na_2CO_3$, which is evidenced by the presence of the two main peaks corresponding to this phase at $2\theta$ = 3.989° (overlapping with a secondary peak of $Na_2TiO_3$) and $2\theta$ = 4.289°. During the first stage of the heating process, a slight increment in the amount of carbonate can be observed, but after reaching 300 °C, it starts to diminish. At 350 °C, no trace of $Na_2CO_3$ can be detected. Between 350 °C and 660 °C, β-$Na_2TiO_3$ is the only phase remaining. This is consistent with the TG results shown in Fig. 4, and also with previously reported curves,[27] in which the absorption of $CO_2$ into similar samples is only observed at temperatures starting from 675 °C. At this temperature, a phase change occurs, evidenced by the subtle appearance of new peaks. Some of these new peaks match the ones observed in the previous measurement, indicating the presence of a $Na_{16}Ti_{10}O_{28}$-like structure. In this case, due to the higher abundance of this phase, it was possible to perform a deeper analysis of the XRD data. A refinement of the final diffractogram (Fig. 8) showed a higher number of sodium and oxygen vacancies compared to the one observed by Sánchez-Camacho *et al.*,[27] indicating a composition more in line with a $Na_{16-2x}Ti_{10}O_{28-x}$ formula, with $x$ in the range 0.1–0.25. This leads to a slightly modified eqn (8) as follows:

$$10Na_2TiO_3 \rightarrow Na_{16-2x}Ti_{10}O_{28-x} + (2 + x)Na_2O \quad (10)$$

By observing Fig. 7, it is clear that a second reaction resulting in the formation of $Na_{0.97}Ti_2O_4$ does not occur. This is difficult to understand since at this stage, the temperature and gas flow conditions are comparable to those in the previous experiment. A possible explanation is that the $CO_2$ gas flow generates a change in the morphology of $Na_2TiO_3$ by preventing the first transition towards the monoclinic phase. These changes then are transferred to $Na_{16-2x}Ti_{10}O_{28-x}$, inhibiting the further decomposition of the titanate. As it can be observed from Fig. 5, reaction (9) is very slow, so it may be possible that an unfavorable particle morphology, such as larger crystallite sizes[33] or larger diffusion paths, could make this reaction impossible to see in the time frame of the experiment. A closer inspection toward the last XRD pattern

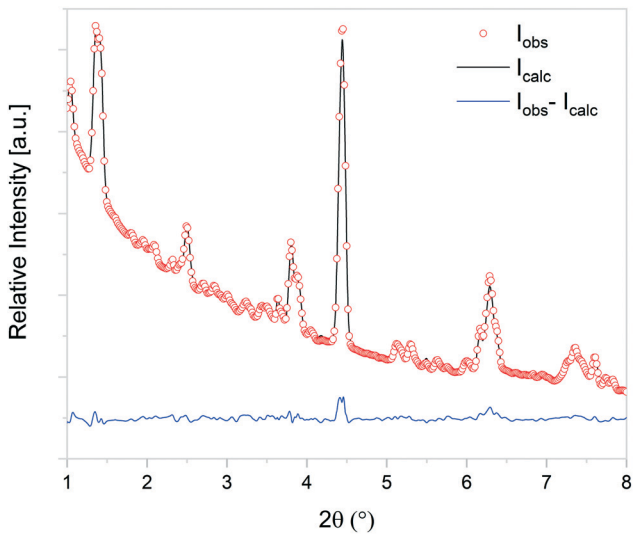


Fig. 8 Observed (open circles) and calculated (line) X-ray diffraction patterns of $Na_{16-2x}Ti_{10}O_{28-x}$, with $x$ in the range 0.1–0.25.

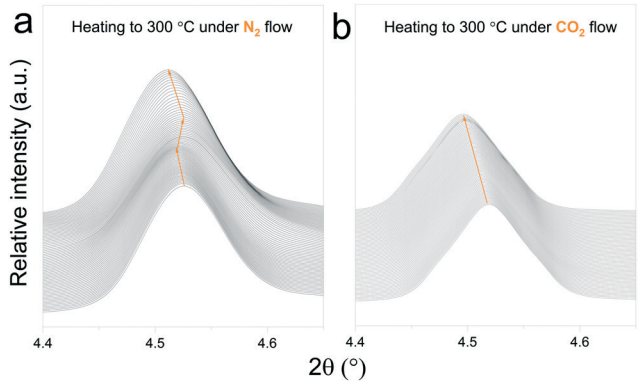


Fig. 9 Structural changes of $Na_2TiO_3$ under dynamic heating at a ramp of 5 °C $min^{-1}$ under a $N_2$ flow (a) and $CO_2$ flow (b).

from these measurements showed a faint hint of the characteristic peak of $Na_{0.97}Ti_2O_4$ at $2\theta = 1.9°$. This different morphology could also be an explanation about why the decomposition into $Na_4Ti_5O_{12}$ and $Na_{4.33}Ti_5O_{12}$ is not observed here, since those two reactions are much slower than the decomposition to $Na_{16-2x}Ti_{10}O_{28-x}$, as can be seen by comparing Fig. 5b and 6b.

### 3.3 Effect of the initial atmosphere on the $Na_2TiO_3$–$CO_2$ reaction pathway

*In situ* X-ray diffraction analysis for real-time monitoring of chemical reactions on $CO_2$ capture materials[15,37–40] has been proven to be a useful tool to understand the behaviour of $CO_2$ sorbents at temperatures that are relevant for real applications, allowing the identification of structural changes, to reveal intermediate phases and re-conversion processes occurring during operational conditions[29,41] and to investigate the impact of the presence of $H_2O$ in the gas stream.[42] However, due to the limited access to powerful X-ray probes, many reports have proposed carbonation mechanisms of these materials based on *ex situ* X-ray diffraction data.[27,43] Typically, *ex situ* samples are obtained after heating different samples under an inert atmosphere, switching the gas flow to $CO_2$ once the desired temperature is reached and then maintaining isothermal conditions for a couple of hours. The results obtained by these procedures can provide valuable insights into the reaction mechanism of $CO_2$ sorbents. However, the results presented in this work indicate that thermal preheating under an inert atmosphere can severely affect the structure of the sorbent prior to its exposure to $CO_2$. In Fig. 9ab and , a selected $2\theta$ region in which $Na_2TiO_3$ is heated under a $N_2$ and $CO_2$ gas flow, respectively, is displayed. From Fig. 9a, it can be observed that there is a transition from monoclinic $Na_2TiO_3$ to β-$Na_2TiO_3$ when the sample is subjected to a $N_2$ flow. As shown in the previous subsection, these structural changes can influence the further dynamic evolution of the material by either slowing or speeding up the next reaction steps. Although these transitions are difficult to observe with traditional methods, they are critical to explain the dynamic $CO_2$ capture thermograms. This further emphasizes the need for *in situ* tools to obtain an accurate description of the $CO_2$ capture performance of sorbent materials.

## 4 Conclusions

$Na_2TiO_3$ was successfully synthesized from NaOH and $TiO_2$ *via* a solid state route, where the powder mixture was heat treated at 800 °C for 5 h. The $CO_2$ sorption properties of synthesized $Na_2TiO_3$ were analyzed by dynamic thermogravimetric analysis.

*In situ* synchrotron XRD analysis, performed to study the reaction mechanism of $Na_2TiO_3$ at high temperatures in the presence of $CO_2$, revealed the complex behaviour of the Na–Ti–O system. With the aim of differentiating phase transformations driven by carbonation processes from those occurring as a consequence of the thermal stability of the ceramic, the high temperature behavior of $Na_2TiO_3$ under different gas flows was studied. A careful analysis of $Na_2TiO_3$ phase transitions showed that its structure can be strongly influenced by the surrounding atmosphere.

At 40 °C, samples subjected to a $N_2$ flow show the presence of β-$Na_2TiO_3$ and monoclinic $Na_2TiO_3$ phases, while the sample subjected to a $CO_2$ flow showed no evidence of the latter. This difference in composition disappears upon heating, when the monoclinic phase reverts to β-$Na_2TiO_3$. Further heating at temperatures above 650 °C causes β-$Na_2TiO_3$ to transition to $Na_{16-2x}Ti_{10}O_{28-x}$. This transition occurs under either a pure $N_2$ or $CO_2$ gas flow. However, at this point, while the samples have reached a similar situation in terms of phase composition and environmental conditions, the previous history of the sample seems to play a role in the kinetic behaviour of the system. In both cases, when subjected to a $CO_2$ flow, $Na_{16-2x}Ti_{10}O_{28-x}$ undergoes a carbonation process. However, although both samples showed similar reaction paths, considerable differences in the reaction kinetics between both have been observed. The retardation effect observed for the sample preheated under $CO_2$ is evident in the results, and it can be attributed to morphological differences related to the lack of transition from the monoclinic phase, which could influence the diffusion processes required for the carbonation of $Na_{16-2x}Ti_{10}O_{28-x}$.

The differences found when subjecting $Na_2TiO_3$ to different atmospheres upon heating demonstrate that *in situ* XRD characterization is essential to monitor in real time the structural changes that occur to the system and to correlate them to dynamic TG observations, providing a much reliable insight on the chemical processes that take place during sorption reactions.

## Conflicts of interest

"There are no conflicts to declare".

## Acknowledgements

The authors thank the European Synchrotron Radiation Facility for in-house beamtime allocation and financial support, and Florian Rusello and Tiago Coutinho for their help with the preparation of the experimental setup. This work was partially supported by CONICET, ANPCyT – (PICT 2018-00606), CNEA and Cuyo University.

## Notes and references

1 O. US EPA, *Global Non-CO2 GHG Emissions: 1990–2030*, 2016, https://www.epa.gov/global-mitigation-non-co2-greenhouse-gases/global-non-co2-ghg-emissions-1990-2030.
2 A. Alonso, J. Moral-Vico, A. Abo Markeb, M. Busquets-Fité, D. Komilis, V. Puntes, A. Sánchez and X. Font, *Sci. Total Environ.*, 2017, **595**, 51–62.
3 Q. Wang, J. Luo, Z. Zhong and A. Borgna, *Energy Environ. Sci.*, 2011, **4**, 42–55.
4 A. Samanta, A. Zhao, G. K. H. Shimizu, P. Sarkar and R. Gupta, *Ind. Eng. Chem. Res.*, 2012, **51**, 1438–1463.
5 J. Wang, L. Huang, R. Yang, Z. Zhang, J. Wu, Y. Gao, Q. Wang, D. O'Hare and Z. Zhong, *Energy Environ. Sci.*, 2014, **7**, 3478–3518.
6 M. G. Plaza, S. Martínez and F. Rubiera, *Energies*, 2020, **13**, 5692.
7 T. O. Nelson, A. Kataria, P. Mobley, M. Soukri and J. Tanthana, *Energy Procedia*, 2017, **114**, 2506–2524.
8 E. R. van Selow, P. D. Cobden, P. A. Verbraeken, J. R. Hufton and R. W. van den Brink, *Ind. Eng. Chem. Res.*, 2009, **48**, 4184–4193.
9 P. Pecharaumporn, S. Wongsakulphasatch, T. Glinrun, A. Maneedaeng, Z. Hassan and S. Assabumrungrat, *Int. J. Hydrogen Energy*, 2019, **44**, 20663–20677.
10 B. Dou, C. Wang, Y. Song, H. Chen, B. Jiang, M. Yang and Y. Xu, *Renewable Sustainable Energy Rev.*, 2016, **53**, 536–546.
11 C. S. Martavaltzi, E. P. Pampaka, E. S. Korkakaki and A. A. Lemonidou, *Energy Fuels*, 2010, **24**, 2589–2595.
12 D. M. D'Alessandro, B. Smit and J. R. Long, *Angew. Chem., Int. Ed.*, 2010, **49**, 6058–6082.
13 Y. Zhang, Y. Gao, H. Pfeiffer, B. Louis, L. Sun, D. O'Hare and Q. Wang, *J. Mater. Chem. A*, 2019, **7**, 7962–8005.
14 Y. Hu, W. Liu, Y. Yang, M. Qu and H. Li, *Chem. Eng. J.*, 2019, **359**, 604–625.
15 M. L. Grasso, M. V. Blanco, F. Cova, J. A. González, P. A. Larochette and F. C. Gennari, *Phys. Chem. Chem. Phys.*, 2018, **20**, 26570–26579.
16 C. Wang, B. Dou, Y. Song, H. Chen, Y. Xu and B. Xie, *Ind. Eng. Chem. Res.*, 2014, **53**, 12744–12752.
17 T. Ávalos Rendón, J. Casa-Madrid and H. Pfeiffer, *J. Phys. Chem. A*, 2009, **113**, 6919–6923.
18 Q. Zheng, L. Huang, Z. Zhong, B. Louis and Q. Wang, *Chem. Eng. J.*, 2020, **380**, 122444.
19 G. Ji, M. Z. Memon, H. Zhuo and M. Zhao, *Chem. Eng. J.*, 2017, **313**, 646–654.
20 R. Rodríguez-Mosqueda and H. Pfeiffer, *J. Phys. Chem. C*, 2013, **117**, 13452–13461.
21 J. Liu, Z. Wang, Z. Wang, J. Song, G. Li, Q. Xu, J. You, H. Cheng and X. Lu, *Phys. Chem. Chem. Phys.*, 2019, **21**, 13135–13143.
22 A. López-Ortiz, N. G. P. Rivera, A. R. Rojas and D. L. Gutierrez, *Sep. Sci. Technol.*, 2005, **39**, 3559–3572.
23 G. Ji, H. Yang, M. Z. Memon, Y. Gao, B. Qu, W. Fu, G. Olguin, M. Zhao and A. Li, *Appl. Energy*, 2020, **267**, 114874.
24 S. Song, M. Kotobuki, Y. Chen, S. Manzhos, C. Xu, N. Hu and L. Lu, *Sci. Rep.*, 2017, **7**, 373.
25 T. Kobayashi, W. Zhao, H. B. Rajendra, K. Yamanaka, T. Ohta and N. Yabuuchi, *Small*, 2020, **16**, 1902462.
26 Q. Liu, Z. Hu, W. Li, C. Zou, H. Jin, S. Wang, S. Chou and S.-X. Dou, *Energy Environ. Sci.*, 2021, **14**, 158–179.
27 P. Sánchez-Camacho, I. C. Romero-Ibarra, Y. Duan and H. Pfeiffer, *J. Phys. Chem. C*, 2014, **118**, 19822–19832.
28 H. Outokumpu, *HSC Chemistry For Windows Version 6.1*, 2009.
29 F. Cova, G. Amica, K. Kohopää and M. V. Blanco, *Inorg. Chem.*, 2019, **58**, 1040–1047.
30 J. Kieffer and D. Karkoulis, *J. Phys.: Conf. Ser.*, 2013, **425**, 202012.
31 M. Wojdyr, *J. Appl. Crystallogr.*, 2010, **43**, 1126–1128.
32 B. H. Toby and R. B. Von Dreele, *J. Appl. Crystallogr.*, 2013, **46**, 544–549.
33 F. Meng, Y. Liu, T. Xue, Q. Su, W. Wang and T. Qi, *RSC Adv.*, 2016, **6**, 112625–112633.
34 M. L. Grasso, P. Arneodo Larochette and F. C. Gennari, *J. CO2 Util.*, 2020, **38**, 232–240.
35 A. Boultif and D. Louër, *J. Appl. Crystallogr.*, 2004, **37**, 724–731.
36 M. Mayer and G. Perez, *Rev. Chim. Miner.*, 1976, **13**, 237–242.
37 R. Molinder, T. P. Comyn, N. Hondow, J. E. Parker and V. Dupont, *Energy Environ. Sci.*, 2012, **5**, 8958–8969.
38 M. T. Dunstan, S. A. Maugeri, W. Liu, M. G. Tucker, O. O. Taiwo, B. Gonzalez, P. K. Allan, M. W. Gaultois, P. R. Shearing, D. A. Keen, A. E. Phillips, M. T. Dove, S. A. Scott, J. S. Dennis and C. P. Grey, *Faraday Discuss.*, 2016, **192**, 217–240.
39 A. Biasin, C. U. Segre and M. Strumendo, *Cryst. Growth Des.*, 2015, **15**, 5188–5201.
40 J. Manuel Valverde, A. Perejon, S. Medina and L. A. Perez-Maqueda, *Phys. Chem. Chem. Phys.*, 2015, **17**, 30162–30176.
41 M. V. Blanco, K. Kohopää, I. Snigireva and F. Cova, *Chem. Eng. J.*, 2018, **354**, 370–377.
42 J. M. Valverde and S. Medina, *Phys. Chem. Chem. Phys.*, 2017, **19**, 7587–7596.
43 F. Durán-Muñoz, I. C. Romero-Ibarra and H. Pfeiffer, *J. Mater. Chem. A*, 2013, **1**, 3919–3925.